Opto-Electronic Advances

Original Article

2023, Vol. 6, No. X

DOI: 10.29026/oea.2023.210163

Carnivorous plants inspired shape-morphing slippery surfaces

Dong-Dong Han[1], Yong-Lai Zhang[1]*, Zhao-Di Chen[1], Ji-Chao Li[1], Jia-Nan Ma[1], Jiang-Wei Mao[1], Hao Zhou[1] and Hong-Bo Sun[2]

Carnivorous plants, for instance, *Dionaea muscipula* and *Nepenthes* pitcher plant, inspired the innovation of advanced stimuli-responsive actuators and lubricant-infused slippery surfaces, respectively. However, hybrid bionic devices that combine the active and passive prey trapping capabilities of the two kinds of carnivorous plants remain a challenge. Herein, we report a moisture responsive shape-morphing slippery surface that enables both moisture responsive shape-morphing and oil-lubricated water repellency for simultaneous active- and passive-droplet manipulation. The moisture deformable slippery surface is prepared by creating biomimetic microstructures on graphene oxide (GO) membrane *via* femtosecond laser direct writing and subsequent lubricating with a thin layer of oil on the laser structured reduced GO (LRGO) surface. The integration of a lubricant-infused slippery surface with an LRGO/GO bilayer actuator endows the actuator with droplet sliding ability and promotes the moisture deformation performance due to oil-enhanced water repellency of the inert layer (LRGO). Based on the shape-morphing slippery surface, we prepared a series of proof-of-concept actuators, including a moisture-response *Dionaea muscipula* actuator, a smart frog tongue, and a smart flower, demonstrating their versatility for active/passive trapping, droplet manipulation, and sensing.

Keywords: femtosecond laser fabrication; graphene oxide; moisture responsive actuators; slippery surface; bionic devices

Han DD, Zhang YL, Chen ZD, Li JC, Ma JN et al. Carnivorous plants inspired shape-morphing slippery surfaces. *Opto-Electron Adv* **6**, 210163 (2023).

Introduction

Carnivorous plants that can trap and digest small insects through sophisticated actuating mechanisms or unique surface wettability have inspired the development of artificial smart surfaces/devices for engineering applications, such as anti-icing surfaces[1], anti-biofouling[2], droplet condensation[3], and droplet manipulation[4,5]. Mimicking their trapping behaviors has led to innovative strategies for designing synthetic surfaces[6], actuators[7,8], and robots[9,10]. Generally, the trapping mechanism of carnivorous plants differs among different species, which can be simply classified into two categories: active trapping and passive trapping[11,12]. *Dionaea muscipula* is a typical example of the former-type carnivorous plants. It snaps prey, for instance, flies and spiders, by closing a couple of lobes within milliseconds under the actuation of slight touches on the trigger hairs[13,14]. Recently, by mimicking the trapping behavior of *Dionaea muscipula*, stimuli-responsive actuators working under various external stimuli (e.g., light, electricity, and temperature) have been successfully developed based on different smart materials. For instance, Han et al. demonstrated a light-re-

[1]State Key Laboratory of Integrated Optoelectronics, College of Electronic Science and Engineering, Jilin University, Changchun 130012, China; [2]State Key Laboratory of Precision Measurement Technology and Instruments, Department of Precision Instrument, Tsinghua University, Beijing 100084, China.

*Correspondence: YL Zhang, E-mail: yonglaizhang@jlu.edu.cn

Received: 30 November 2021; Accepted: 9 March 2022 ; Published online: 25 August 2022

sponsive *Venus* flytrap bilayer actuator using Au nanorods and graphene as a photothermal layer[15]; Kim et al. fabricated a bilayer photothermally foldable *Venus* flytrap by using tosylate doped poly(3,4-ethylenedioxythiophene) (PEDOT) as a photothermal layer[16]; Zhu et al. reported a *Dionaea muscipula* inspired electrothermal actuator using laser reduced GO as a conductive layer[17]. To mimic their trapping behavior, artificial actuators should have stimuli-responsive deformation ability, large trapping force, and a very short response time simultaneously to avoid the escape of insects. However, the rapid closure (snapping) of the reported Dionaea muscipula-inspired actuators is far from natural ones (within milliseconds, ~100 ms)[18–21], limiting their practical applications. The representative example of the latter type is the *Nepenthes* pitcher plant. The microstructures at the pitcher's rim enable directional water transport from the interior, forming a water-lubricated slippery surface[22,23]. When the prey steps on the pitcher's rim, it cannot adhere to the surface and have to slide down into digestive juices. Inspired by the *Nepenthes* pitcher plant, Wong et al. first reported an advanced liquid-infused porous surface that repels oils on the feet of insects[24]. The resultant slippery surface demonstrated stable liquid repellency, self-healing ability, and optical transparency. Gulfam et al. successfully developed phase-change slippery liquid-infused porous surfaces with thermo-responsive wetting and shedding states[25]. Subsequently, liquid-lubricated slippery surfaces have been successfully developed based on different substrates, including organogel[26], graphene sponge[27], metal mesh[28], magnetic microcilia surface[7], and micropillar arrayed metal oxides[29]. Significantly, Lv et al. comprehensively summarized recent advances and developments on bioinspired SLIPSs and wettability gradient surfaces, focusing on their synergistic cooperation for condensation and fluid transport related applications[30,31]. To date, with the rapid advances of material science and nanotechnologies, various robotic systems and synthetic smart surfaces have been successfully developed by mimicking the *Dionaea muscipula* and *Nepenthes* pitcher plant, respectively[32–34]. However, hybrid bionic devices that combine the merits of the two distinct kinds of carnivorous plants, with both positive and passive trapping abilities, are still rare. Obviously, the combination of *Dionaea muscipula* inspired actuators with slippery surface that mimics *Nepenthes* pitcher plant are of benefit to both actuator design and the development of smart surface with superwettability. Nevertheless, it is challenging to reach this end.

Herein, inspired by carnivorous plants, we report a moisture responsive shape-morphing slippery surface that combines hybrid working mechanisms of both the *Dionaea muscipula* and *Nepenthes* pitcher plant. Femtosecond laser direct writing (FsLDW) induced photoreduction and simultaneous structuring was employed to prepare a GO and LRGO bilayer actuator that enables dynamic deformation under moisture actuation. After that, a lubricant-infused slippery surface was integrated with the graphene actuator by immobilizing lubricant at the LRGO side through the capillary forces. In this way, a hybrid bionic surface with moisture responsive shape-morphing ability and lubricant-infused slippery wettability has been created. As a proof-of-concept demonstration, the moisture responsive shape-morphing slippery surface has been tailored into various device structures, which were further used for active/passive trapping, droplet collection, droplet manipulation, and rainfall sensing.

Results and discussion

Figure 1 shows the basic concept of stimuli-responsive shape-morphing slippery surfaces that combine the hybrid working mechanisms of the *Dionaea muscipula* and *Nepenthes* pitcher plant. The two types of carnivorous plants demonstrate distinct strategies for trapping prey, in which *Nepenthes* pitcher plant catches insects through a passive trapping mechanism with the help of lubricants-infused slippery surface. In contrast, *Dionaea muscipula* performs an active trapping behavior through a sophisticated actuating mechanism. The concept of the hybrid bionic model is the combination of the two tapping behaviors within one synthetic smart surface here, which we call stimuli deformable slippery surface.

To create a slippery surface, the LRGO surface was lubricated by infusing soybean oil into the porous structures. Compared with the frequently-used lubricant, such as FC-70 (~120 $mm^2\ s^{-1}$), Krytox®103 (~82 $mm^2\ s^{-1}$), silicone oil (~50 $mm^2\ s^{-1}$), the soybean oil shows much lower kinematic viscosity (~27.5 $mm^2\ s^{-1}$)[24,35]. The lower kinematic viscosity benefits the lubrication process (Fig. S1). Compared with silicone oil (density, 0.965 –0.972 g/mL)[36,37], the soybean oil has lower density (0.916–0.921 g/mL)[38,39]. In this regard, the resultant surface based on soybean oil would be lighter, facilitating bending deformation. In addition, the soybean oil that is derived from natural beans is non-toxic and biocompatible,

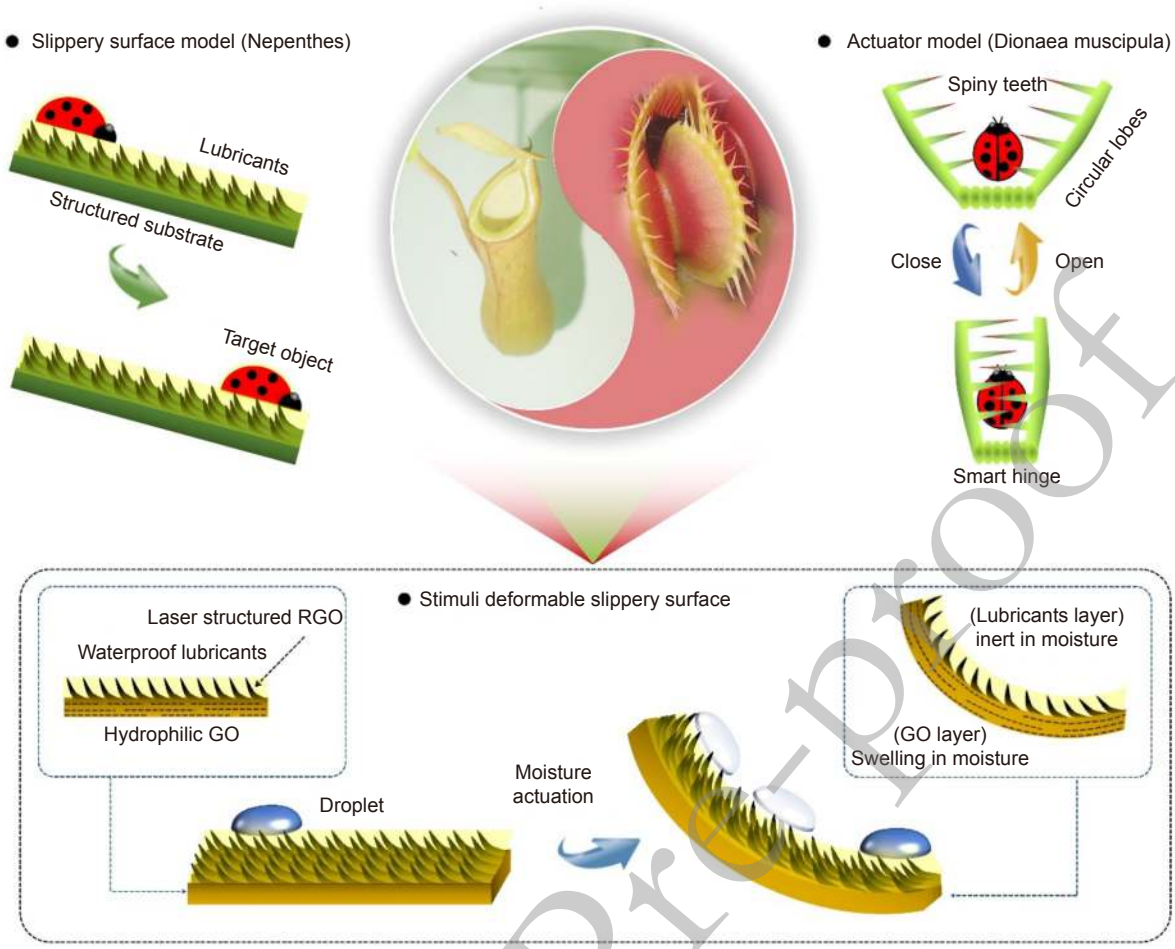

Fig. 1 | Basic concept of hybrid bionic moisture responsive shape-morphing slippery surface inspired from multi-form carnivorous plants. The Nepenthes pitcher plant catches insects passively with the help of a lubricant-infused slippery surface. The Dionaea muscipula preys actively through a stimuli-responsive actuation mechanism. We combined the slippery surfaces (passive prey) and stimuli-responsive actuation (active prey), so we proposed a hybrid bionic moisture deformable slippery surface-based GO, which enables both active and passive droplet manipulation. GO: graphene oxide; RGO, reduced GO.

which is much suitable for prey trapping. Considering the low density, non-toxicity, and biocompatibility, we chose soybean oil in this work.

The detailed fabrication procedure of the moisture responsive shape-morphing slippery surface based on GO was illustrated in Fig. 2(a). First, femtosecond laser direct writing was employed to create *Nepenthes*-inspired microstructures on the GO surface (Fig. S2). The laser spots size (radius) is 2.15±0.25 μm, and the laser fluence is ~1.38 J/cm^2, measured according to the reference[40,41]. After laser structuring and reduction, most of the oxygen-containing groups (OCGs) can be removed due to the photoreduction effect, including the electronic excitation effect and the electron-hole recombination-induced thermal effect[42–44]. Nevertheless, considering the limited light penetration and the suppressed thermal relaxation, the photoreduction and the simultaneous structuring only occurred at the surface of a GO membrane. Consequently, an LRGO/GO bilayer structure formed naturally through this self-controlled laser reduction. Subsequently, lubricants were infused into the LRGO through capillary force due to the presence of laser exfoliated nanostructures. A moisture-responsive actuator with a lubricant-infused slippery surface was prepared.

To make a clear comparison of the microstructures between the peristome of the *Nepenthes* pitcher plant and the LRGO surface, we characterized the natural prototype and the LRGO sample by scanning electron microscope (SEM). Initially, the GO surface is flat with randomly distributed wrinkles (Fig. S3). Figure 2(b) shows the SEM image of the *Nepenthes* pitcher plant's peristome, a hierarchical microstructure made of overlapped epidermal cells. The *Nepenthes* pitcher plant utilizes its distinct hierarchical structure in the peristome to

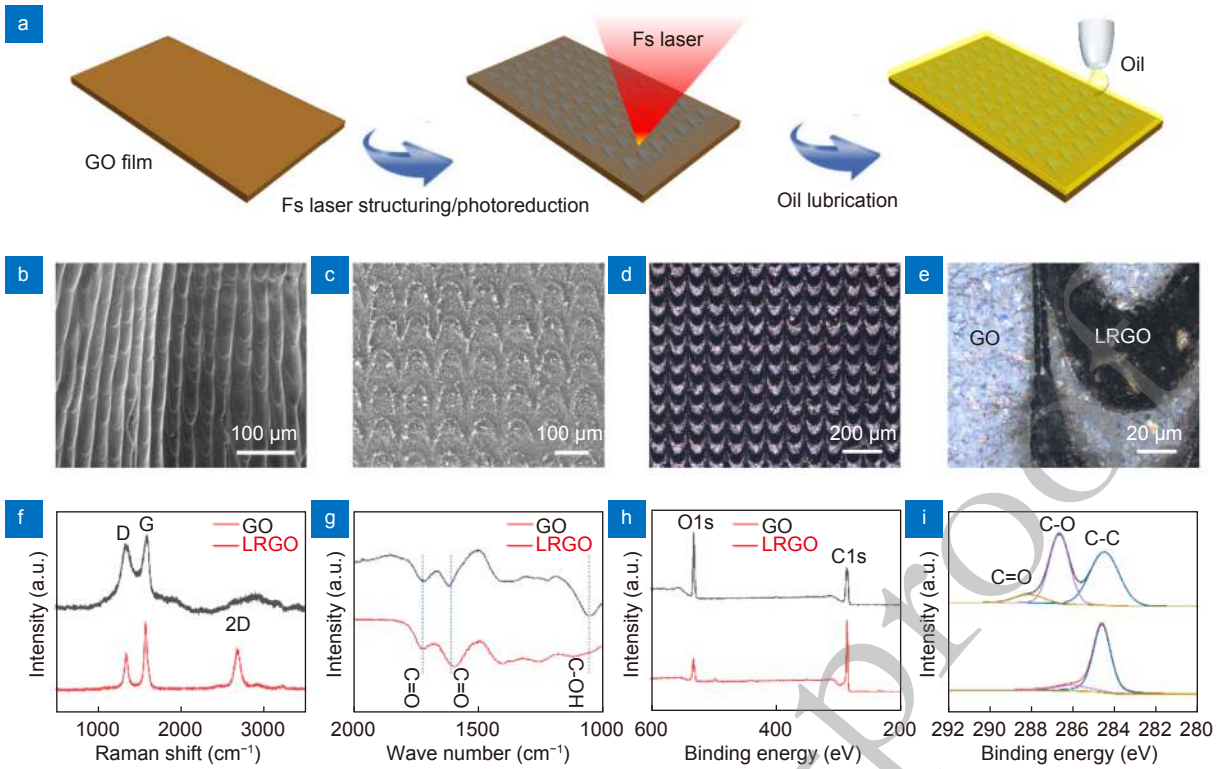

Fig. 2 | Fabrication, morphology, and element characterization of the moisture responsive shape-morphing slippery surface. (**a**) Fabrication processing of the moisture responsive shape-morphing slippery surface. A femtosecond (fs) laser was used to reduce GO and induce microstructures similar to the *Nepenthes* pitcher plant. A waterproof lubricant was infused into the LRGO surface to form the slippery surface. (**b**) The scanning electron microscope (SEM) image of the *Nepenthes* pitcher plant. (**c**) The SEM image of the LRGO surface. (**d**, **e**) The confocal laser scanning microscope (CLSM) images of the LRGO. (**f**) The Raman spectra, (**g**) Fourier transform infrared (FTIR) spectra, (**h**) X-ray photoelectron spectroscopy (XPS) survey spectra, and (**i**) C1s XPS spectra of the GO and LRGO sides of the bilayer actuator.

transport nectar or rainwater directionally, forming the stable liquid-infused surface. In this work, we focused on the oil lubrication effect rather than the directional liquid transport property, so we fabricated a similar pattern of a porous structure without controlling the height of the patterns. Figure 2(c) is the SEM image of the LRGO surface. Using the FsDLW patterning, we can fabricate similar microstructures on GO *via* laser-induced photoreduction. The as-formed LRGO structure is comparable to that of the peristome of the *Nepenthes* pitcher plant (Fig. 2(d)), and LRGO patterns can be clearly identified through confocal laser scanning microscope (CLSM) image (Fig. 2(e)). The width is ~90 μm; the spacing is ~8 μm; the height is ~10 μm.

Additionally, we investigated the surface chemical composition of LRGO and compared it with that of GO (the backside of the film). After laser reduction, the water contact angle (CA) of the RGO is ~93°, and the oil CA of the RGO is ~5° (Fig. S4), which demonstrates that the RGO is hydrophobic and oleophilic. Raman spectra of the GO side show typical G and D bands, indicating the sp^2 carbon network and the presence of abundant defects. After femtosecond laser treatment, the LRGO sample shows an increased G band peak and the presence of a 2D peak, indicating the removal of OCG defects and the recovery of graphene networks. Fourier transform infrared (FTIR) spectra also confirm the photoreduction of GO, in good agreement with the Raman spectra. Transmission bands corresponding to OCGs, C=O, and C–OH, are much richer at the GO side than on the LRGO side. X-ray photoelectron spectroscopy (XPS) spectra show that the oxygen signal of LRGO decreased remarkably due to deoxygenation. The C/O atom ratios for GO and LRGO are 2.25 and 5.92, respectively. C1s spectra of LRGO show that the carbon bonded to oxygen in the forms of C–O at 286.8 eV (hydroxyl and epoxy carbon) and C=O at 288.1 eV (carbonyl) decreased remarkably after femtosecond laser reduction. The distinct surface chemical composition of the two sides benefits the moisture-responsive deformation behavior of the LRGO/GO bilayer.

To evaluate the slippery properties, we first investigated

the surface wettability and droplets sliding behavior. The surface tension of water and soybean oil is ~72 and ~33.57 mN/m, respectively. The interfacial tension between water and soybean oil is ~30.9 mN/m. According to reference[45], the lubricant (oil) will cloak the water droplet. Therefore, the oil removal with the shedding droplet may result in the lost of oil, which consequently affects its low adhesion properties. Nevertheless, this issue can be improved by using lubricant with higher oil-water interfacial tension. Figure 3(a) shows the slippery model on a tilted slippery surface. To verify the liquid repellency, the water (5 μL) CA on the slippery surface was measured to be ~62°, and the sliding angle (SA) was only ~3° (Fig. 3(b)). The advancing and receding CAs are 64° and 61°, respectively (Fig. S5). GO surface is hydrophilic, and the CA is ~42°. A trail of fluorochrome was observed after the water droplet slid on the surface of GO (Fig. S6). Sliding occurred without leaving behind a fluorochrome trail (50 μL, Fig. 3(c); Movie S1). The size of the droplet in terms of radius along with the volume is above the capillary length. Generally, the capillary length can be calculated according to the following equation:

$$l_c = (\gamma/\rho g)^{1/2},$$

where l_c, capillary length; γ, surface tension of liquid; ρ, density; g, gravitational acceleration. Accordingly, the capillary length of water was ~ 2.7 mm. In this work, the

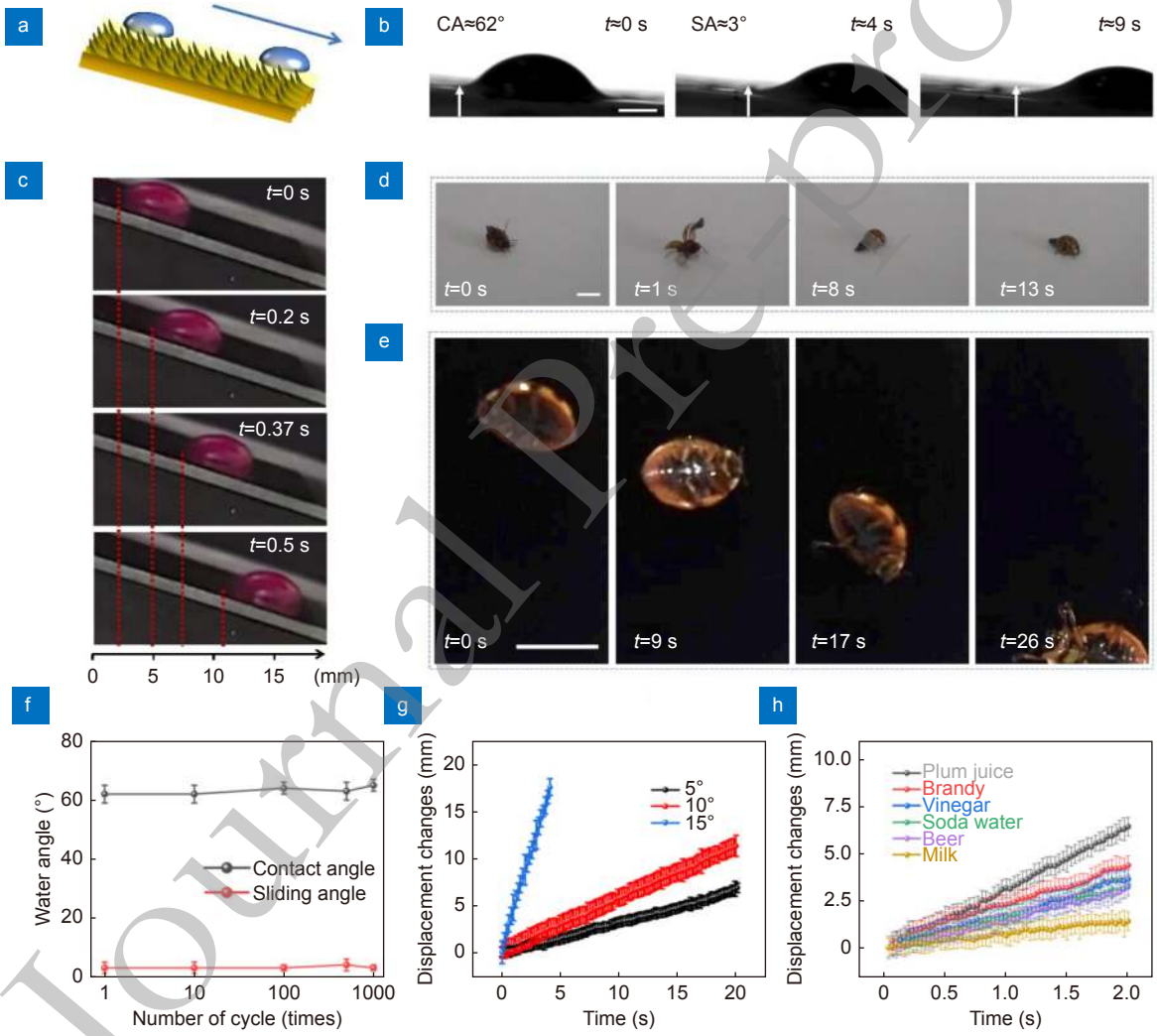

Fig. 3 | The properties of the lubricant-infused slippery surface. (**a**) Schematic illustration of the water droplet sliding behavior. (**b**) The lubricant-infused slippery surface's water contact angle (CA) and sliding angle (SA). The scale bar is 1 mm. (**c**) The photographs of a droplet (R6G labeled) sliding behavior on a tilted surface. (**d**) The overturning behavior of a ladybird on a general paper surface. The scale bar is 5 mm. (**e**) The overturning and sliding behavior of a ladybird on our lubricant-infused slippery surface. The scale bar is 5 mm. (**f**) The durability of CA and SA on oil-infused LRGO surface for 1000 cycles. (**g**) Sliding displacement of a water droplet vs. time. The tilted angles θ = 5°, 10°, and 15°, respectively. (**h**) The sliding behavior of various liquid droplets on our lubricant-infused slippery surface. The tilted angle θ = 30°.

radius of water droplets exceed this value, and thus the gravity at the interface drives the sliding of the droplets. The Furmidge equation[46–48] could be used to describe the force balance and infer the smallest droplet size for what this configuration would work (Fig. S7). Furthermore, no staining was observed on the slippery surface, indicating the good water-repelling property. In our experiment, we also tested the slippery behavior of a live ladybird on our slippery surface and further compared it with that on a general paper of the same inclination. As shown in Fig. 3(d) and 3(e), the ladybird overturned can turn over easily on the paper surface due to the surface roughness. On the contrary, it cannot turn over and rapidly slide down the slippery surface.

To quantitatively measure the slippery performance, when the lubricant-infused slippery surface was inclined by only 3°, the water droplet released on it can slide away with good durability of sliding performance for 1000 cycles (Fig. 3(f)). Then, we tilted the surface by 5°, 10°, and 15°, respectively, and recorded the water droplet (100 μL) displacement changes over time (Fig. 3(g)). Notably, the water droplet displacement shows a linear dependence on time with different titled angles, indicating a uniform slippery speed and good stabilities (Fig. S8). The average velocity of a water droplet is 0.34±0.03, 1.77±0.2, 4.29±0.5 mm/s when the tilted angle is 5°, 10°, and 15°, respectively. In addition to a water droplet, slippery surfaces can also slide common liquid droplets (100 μL) in our daily lives, such as plum juice, brandy, vinegar, soda water, beer, and milk (Fig. 3(h); Fig. S9). The slippery properties endow the lubricant-infused LRGO surface with functionalities similar to the *Nepenthes* pitcher plant.

In addition to the slippery properties, we also studied the LRGO/GO bilayer actuator's performances (Fig. 4(a), Fig. S10). Generally, GO features plenty of OCGs in the form of hydroxyl, epoxy, and carboxyl groups, and the oxygen content is as high as ~30.75% (XPS results).

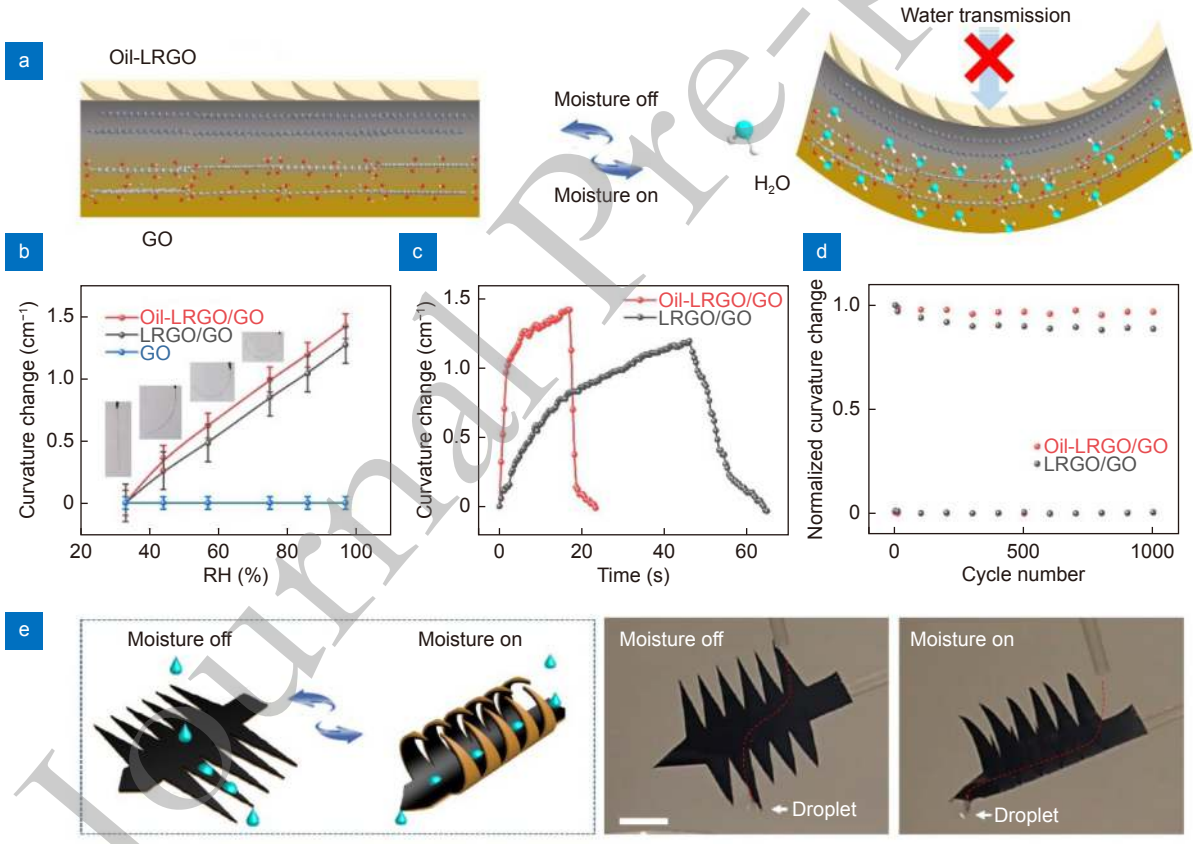

Fig. 4 | Moisture-response deformations of the oil-LRGO/GO actuator. (**a**) Schematic illustration of the moisture responsive shape-morphing mechanism. Under the moisture actuation, water molecules are selectively adsorbed by the GO layer, which leads to the swelling of the GO side. The strain mismatch induces bending deformation. (**b**) Curvature-RH curves of the oil-LRGO/GO, LRGO/GO, and GO films on RH. (**c**) Responsive/recovery properties of the oil-LRGO/GO and LRGO/GO actuator. (**d**) The stability of the oil-LRGO/GO and LRGO/GO actuator for cycling use (1000 times). (**e**) The moisture-response *Dionaea muscipula* actuator with a slippery inner surface. The left scheme is the working model. The right images are the photographs of the deformation and droplet sliding behavior of the *Dionaea muscipula* actuator. The scale bar is 2 cm.

According to the previous theoretical and experimental results and other groups[49–51], such OCGs can interact with water molecules by forming hydrogen bonds. More importantly, with an average interlayer spacing of ~1 nm, GO has been proven a quantum-confined-superfluidics (QSF) system for ultrafast water adsorption and transmission. Therefore, GO is quite sensitive to humidity. The GO film adsorbs water molecules and swells in response to moisture, as evidenced by the increased interlayer spacing upon water adsorption. Nevertheless, in the case of LRGO, most of the OCGs have been removed after laser treatment. Consequently, the interaction between the graphene sheets and water molecules is relatively weak Van der Waals force. Generally, when the LRGO/GO bilayer film is exposed to moisture, water molecules are preferentially adsorbed by the GO layer, which generates a strain mismatch at the bilayer interface and leads to deformation towards the LRGO side. Also, the side and bottom (the GO layer) need to be exposed to relative humidity for the bending to happen, which may limit the applications.

The moisture-induced curvature changes of LRGO/GO and oil-infused LRGO/GO (oil-LRGO/GO) ribbons (12 mm × 1 mm in size) on relative humidity (RH) were investigated and compared with that of a solo film. When the surface is actuated, the moisture is among RH=33% and RH=97%. The oil-LRGO/GO bends in response to moisture changes. With the increase of environmental RH from 33% to 97% (Fig. 4(b)), the curvatures increase from 0 to 1.4 cm^{-1}. The detailed mechanisms for performance improvement are described in Supplementary information Section 3. The relatively larger deformation degree of oil-LRGO/GO than that of LRGO/GO can be attributed to the presence of the oil layer. Essentially, the moisture deformation property can be attributed to the different water adsorption capacity of GO and LRGO layers. When the LRGO surface was lubricated by oil, water absorption within the LRGO layer (inert layer) would be completely prevented. In this case, the moisture deformation property would be further promoted. As a control experiment, the deformation of a solo film is undetectable. In addition to the deformation degree, the presence of the oil layer also promotes the response to moisture. As shown in Fig. 4(c), the response/recovery time for oil-LRGO/GO actuator is ~7.9 s and 6 s, respectively, much smaller than that of the LRGO/GO actuator (34 s and 13.6 s). We tested the bending curvature changes by prolonged exposure to moisture. The bending curvature almost keeps a constant value after exposure to high humidity for 30 minutes, indicating good stability (Fig. S11). Direct contact of a water droplet with the oil-infused side would not change the surface response because the oil layer can effectively repel the droplet, whereas the contact of water with the GO side would wet the surface because GO is very hydrophilic. In this regard, only if the GO surface becomes dry again the moisture responsive properties can be recovered. Notably, both two actuators show good stability for cycling use. After 100 cycles, there is only ~2% drop in the curvature change for the oil-LRGO/GO actuator (Fig. 4(d)). The laser processing parameters used in this work is an optimized result. To prepare the slippery surface, a porous RGO layer is essential. Generally, under laser treatment with low intensity, the reduction effect is unobvious. On the contrary, laser treatment at high intensity would induce the ablation. To create a highly porous structure, the GO surface should be treated at a moderate laser intensity. More importantly, to form a bilayer structure, the GO membrane cannot be fully reduced or ablated. In this case, the laser intensity plays a very important role in the fabrication of this shape-morphing slippery surface. Here, both the laser intensity and the structure geometry can influent the performance of the resultant shape-morphing slippery surface. So it is possible to create better shape-morphing slippery surfaces with optimized characteristics by changing the laser parameters[15,52,53] or structure geometry[2,45,54].

As shown in the Fig. S12(a), the sliding angles of water droplets on the liquid-infused surface along different directions (+*Y*, -*Y*, *X*) are ~3°, 5°, and 10°, respectively, indicating the anisotropic droplet sliding behavior. For moisture responsive deformation, the pattern also plays an important role. We have tested the bending behavior of a ribbon with patterns along with *X* and *Y* directions (Fig. S12(b) and S12(c)). The ribbon prefers to bend along the *Y* direction, suggesting anisotropic deformation. In this regard, the patterning of LRGO would enable better control over droplet sliding and moisture-triggered bending performance.

As control experiments, we also prepared an oil-infused LRGO/GO film without patterning and an oil-coated GO film without reduction for comparison. As shown in Fig. S13, reducing whole GO without patterning would also form a liquid-infused slippery surface, and water droplets can slide on the oil-LRGO surface freely (Fig. S13(a), SA ~3°). But it lost the anisotropic

droplet sliding and the anisotropic deformation properties due to the isotropic structures. On the other hand, just having an oil layer without reduction can cause unobvious deformation under moisture actuation because the liquid layer cannot afford the stress mismatch at the oil-GO interface. Moreover, GO is hydrophilic. Due to the lack of porous structure, it cannot form an oil-infused slippery surface at all (Fig. S13(b) and S13(c)).

Interestingly, the oil-LRGO/GO film can be shaped into various geometries by simple cutting (Fig. S14), revealing the potential for tractable processing. To demonstrate the hybrid bionic models (*Dionaea muscipula* and *Nepenthes* pitcher plant), we fabricated a moisture-responsive *Dionaea muscipula* actuator with an oil-infused LRGO slippery surface (Fig. 4(e); Fig. S15). Under the ambient condition, the spiny teeth array along the two sides open, forming a flat pattern. In this case, the droplets falling on the surface would slide away from the tip of the teeth. When the environmental humidity increased, the *Dionaea muscipula* actuator closed its spiny teeth along the central axis of symmetry. Consequently, the droplets would slide away from the central top tip. Relative photographs show the deformation of the actuator under moisture actuation and the sliding behavior of droplets at different conditions.

Traditional stimuli-responsive actuators enable reversible deformation under external stimuli, revealing the great potential for developing trapping robots. However, in most cases, simple bending deformation is incapable of trapping insects because of the slow response to environmental stimuli or the lack of surface wettability control. We combined the moisture-responsive actuator with a lubricant-infused slippery surface together. The cooperative effect of actuation and slippery property endows the oil-infused LRGO/GO film with enhanced trapping ability. We demonstrated a moisture-responsive shape-morphing slippery surface that can contact droplets actively and let them slide away passively. Based on this hybrid bionic concept, a smart frog tongue that can catch and manipulate droplets containing live tubificidaes is prepared (Fig. 5(a) and 5(b)). Notably, the slippery surface can bend under moisture actuation, get in

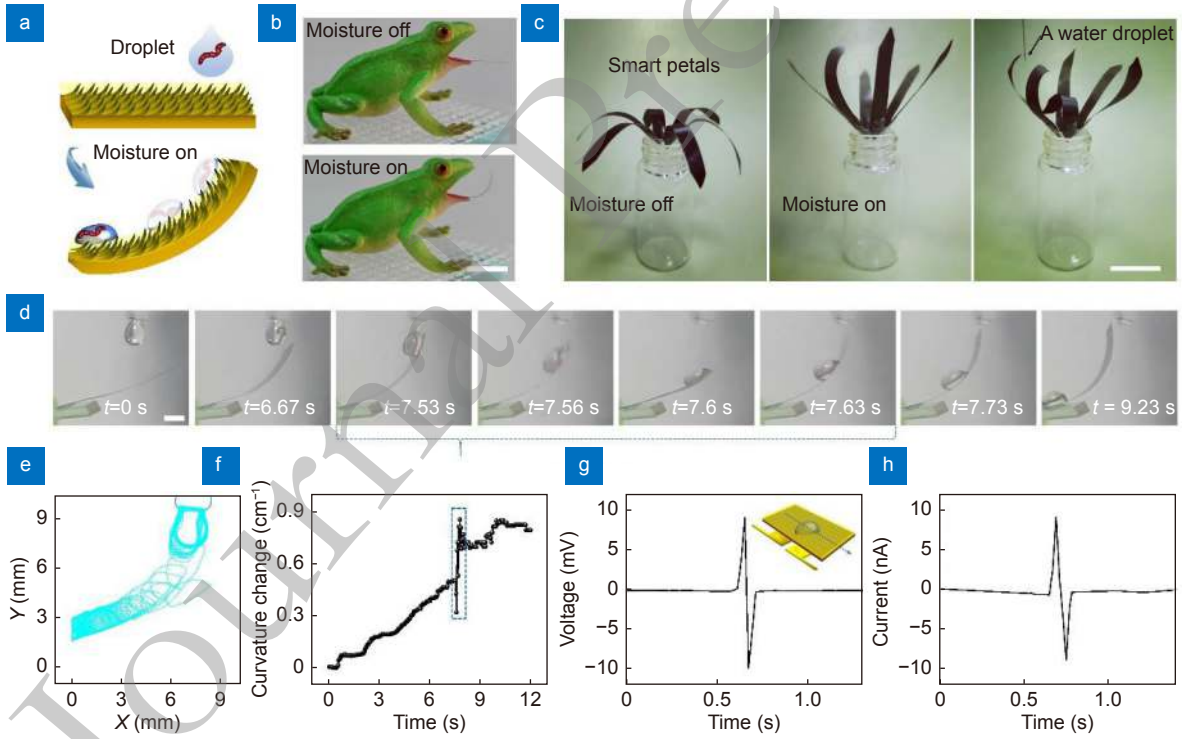

Fig. 5 | The manipulation of droplets on moisture responsive shape-morphing slippery surface. (**a**) Schematic illustration for the active and passive manipulation of a droplet containing live tubificidaes using the shape-morphing slippery surface. (**b**) The photographs of shape-morphing slippery frog tongue. The scale bar is 1.5 cm. (**c**) A smart water droplet harvesting flower. Every flower petal is made of the shape-morphing slippery surface (oil-LRGO/GO). The scale bar is 1.5 cm. (**d**) Moisture triggered active approach to water droplets containing live tubificidaes and the passive sliding behavior on the shape-morphing slippery surface. The scale bar is 0.5 cm. (**e**) The corresponding trajectory of the water droplet peripheries during the dynamic process. (**f**) The curvature changes of the shape-morphing slippery surface in (d). (**g**) The open-circuit voltage and (**h**) short-circuit current.

touch with the droplet, and let it slide to the bottom side, demonstrating both active catching and passive trapping capabilities. In addition to the smart frog tongue, we also prepared a moisture-responsive flower with six deformable and slippery petals at the bottleneck for active droplet harvesting (Fig. 5(c)). When the environmental humidity is low, the flower is in full bloom, exposing the slippery surface to the environment. With the increase of moisture, the petals bend towards the center. The bending behavior and the slippery surface make it possible to transport droplets to the bottle.

The dynamic process of the droplet manipulation, including the active droplet catching and the passive droplet sliding, was demonstrated in Fig. 5(d) (Movie S2). The moisture deformable slippery surface approaches the liquid droplet that contains live tubificidaes by bending itself under moisture actuation. It contacts the droplet within ~7 s; then, the droplet departs from the syringe and slides to the bottom in another 2 s. The displacement of the droplet boundary is shown in Fig. 5(e). As soon as the moisture deformable slippery surface captured the droplet, it dropped down due to gravity (~30 mg). Nevertheless, the whole shape-morphing slippery membrane (25±5 μm in thickness) is strong enough to bear the weight of a droplet and accomplish the droplet sliding, indicating the mechanical robustness and the large deforming force. The corresponding curvature changes of the film on time are displayed in Fig. 5(f). The curvature gradually increases with time and keeps unchanged after 10 s, in which the sudden change in curvature at ~7.5 s can be attributed to the release of the droplet from the syringe.

In addition to the droplet manipulation, this moisture-responsive shape-morphing slippery surface shows the potential applications in droplet detecting by the triboelectricity effect[55]. In this work, the purpose of integrating the triboelectric effect with the shape-morphing slippery surfaces is droplet detection rather than power generation. It enables sensitive detection of the droplet sliding behavior on the shape-morphing slippery surfaces, which is quite helpful for droplet manipulation. The main challenge lies in that the integration of triboelectric devices should not affect the slippery wettability and the moisture responsive shape morphing properties. As a result, the triboelectric performance is not remarkable for electricity generation. A pair of Au electrodes were deposited on the GO side to detect the electrical signals. The lubricant layer of the slippery surface has been employed as an actively deformable slippery substrate for droplet sliding and a dielectric layer for efficient charge transfer. As shown in Fig. 5(g) and 5(h), electrical signals can be detected when droplets slide over the front and rear electrodes. The triboelectric effect-induced electrical signal can be explained as follows: Initially, the potential between two Au electrodes is equivalent, and there is no potential difference between the two Au electrodes. When the droplet slides from the front electrode to the rear electrode, a charge can be induced on the front gold electrode due to the formation of the electric double layer, causing the increase of potential difference.

Conclusions

Inspired by carnivorous plants, such as *Dionaea muscipula* and *Nepenthes* pitcher plants, we fabricated a shape-morphing slippery surface with hybrid bionic functionalities of moisture responsive deformation and oil-lubricated water repellency for active and passive droplet manipulation. FsLDW technology has been employed to create microstructures that mimic the peristome of *Nepenthes* pitcher plant on a film through a photoreduction effect, forming an LRGO/GO bilayer structure. After that, a lubricant layer was infused into the LRGO surface through the capillary forces. In this way, a moisture responsive bilayer actuator has been successfully integrated with a lubricant-infused slippery surface (SA ~3°). Significantly, the in-situ integration of the lubricant-infused slippery surface with the bilayer actuator does not degrade the actuating performance but also improves its deformation degrees under moisture actuation because the presence of an oil layer can entirely prevent the transmission of water molecules through the LRGO side and selective water adsorption only occurs within the GO layer. As a result, the oil-LRGO/GO actuator demonstrated large deformation curvature (1.4 cm^{-1}), short response/recovery time (7.9 s and 6 s, respectively), and improved stability (only ~2% drop after 100 cycles). We demonstrated several actuators that can actively manipulate droplets based on the oil-LRGO/GO film, including a moisture-response Dionaea muscipula actuator, a smart frog tongue, and a smart flower. For practical applications, laser interference ablation that uses interference effect for periodical patterning is a more effective method. Laser inference patterning would be more suitable for large-scale and high-efficient production of shape-morphing slippery surfaces[56,57]. The significance of this work lies in that we fabricated a shape-morphing

slippery surface with hybrid bionic functionalities of both stimuli-responsive deformation and oil-lubricated slippery properties. The combination of shape-morphing ability with the slippery surface benefits both actuating performance and the usefulness of a smart surface with superwettability. Moreover, it leads to new applications beyond target insect trapping, for instance, droplet collection, droplet manipulation, and rainfall sensing. The liquid-infused surfaces have been exploited for their characteristic features such as self-cleaning, self-healing, anti-icing, and anti-biofouling. Moisture-responsive actuators can directly harness energy from naturally occurring or engineered evaporation from water and subsequently convert it to mechanical energy or electricity, such as weather-responsive architectural systems, smart textiles, and soft robots. The cross-species bio-inspired materials benefit both actuator design and the development of smart surfaces with superwettability, and the moisture responsive shape-morphing slippery surface reveals great potential for developing bionic robots.

References

1. Kreder MJ, Alvarenga J, Kim P, Aizenberg J. Design of anti-icing surfaces: smooth, textured or slippery. *Nat Rev Mater* **1**, 15003 (2016).
2. Peppou-Chapman S, Hong JK, Waterhouse A, Neto C. Life and death of liquid-infused surfaces: a review on the choice, analysis and fate of the infused liquid layer. *Chem Soc Rev* **49**, 3688–3715 (2020).
3. Park K C, Kim P, Grinthal A, He N, Fox D et al. Condensation on slippery asymmetric bumps. *Nature* **531**, 78–82 (2016).
4. Villegas M, Zhang YX, Abu Jarad N, Soleymani L, Didar TF. Liquid-infused surfaces: a review of theory, design, and applications. *ACS Nano* **13**, 8517–8536 (2019).
5. Zhao YZ, Su YL, Hou XY, Hong MH. Directional sliding of water: biomimetic snake scale surfaces. *Opto-Electron Adv* **4**, 210008 (2021).
6. Liu XQ, Bai BF, Chen QD, Sun HB. Etching-assisted femtosecond laser modification of hard materials. *Opto-Electron Adv* **2**, 190021 (2019).
7. Cao MY, Jin X, Peng Y, Yu CM, Li K et al. Unidirectional wetting properties on multi-bioinspired magnetocontrollable slippery microcilia. *Adv Mater* **29**, 1606869 (2017).
8. Wong WSY, Li MF, Nisbet DR, Craig VSJ, Wang ZK et al. Mimosa origami: a nanostructure-enabled directional self-organization regime of materials. *Sci Adv* **2**, e1600417 (2016).
9. Li DF, Liu C, Yang YY, Wang LD, Shen YJ. Micro-rocket robot with all-optic actuating and tracking in blood. *Light Sci Appl* **9**, 84 (2020).
10. Jin GX, Hu XY, Ma ZC, Li CH, Zhang YL et al. Femtosecond laser fabrication of 3D templates for mass production of artificial compound eyes. *Nanotechnol Precis Eng* **2**, 110–117 (2019).
11. Ellison AM, Gotelli NJ. Evolutionary ecology of carnivorous plants. *Trends Ecol Evol* **16**, 623–629 (2001).
12. Jürgens A, Sciligo A, Witt T, El-Sayed AM, Suckling DM. Pollinator-prey conflict in carnivorous plants. *Biol Rev* **87**, 602–615 (2012).
13. Suda H, Mano H, Toyota M, Fukushima K, Mimura T et al. Calcium dynamics during trap closure visualized in transgenic venus flytrap. *Nat Plants* **6**, 1219–1224 (2020).
14. Volkov AG, Adesina T, Markin VS, Jovanov E. Kinetics and mechanism of *Dionaea muscipula* trap closing. *Plant Physiol* **146**, 323–324 (2008).
15. Han B, Zhang YL, Zhu L, Li Y, Ma ZC et al. Plasmonic-assisted graphene oxide artificial muscles. *Adv Mater* **31**, 1806386 (2019).
16. Lim H, Park T, Na J, Park C, Kim B et al. Construction of a photothermal venus flytrap from conductive polymer bimorphs. *NPG Asia Mater* **9**, e399 (2017).
17. Zhu L, Gao YY, Han B, Zhang YL, Sun HB. Laser fabrication of graphene-based electrothermal actuators enabling predicable deformation. *Opt Lett* **44**, 1363–1366 (2019).
18. Forterre Y, Skotheim JM, Dumais J, Mahadevan L. How the venus flytrap snaps. *Nature* **433**, 421–425 (2005).
19. Lunni D, Cianchetti M, Filippeschi C, Sinibaldi E, Mazzolai B. Plant-inspired soft bistable structures based on hygroscopic electrospun nanofibers. *Adv Mater Interfaces* **7**, 1901310 (2020).
20. Must I, Sinibaldi E, Mazzolai B. A variable-stiffness tendril-like soft robot based on reversible osmotic actuation. *Nat Commun* **10**, 344 (2019).
21. Taccola S, Greco F, Sinibaldi E, Mondini A, Mazzolai B et al. Toward a new generation of electrically controllable hygromorphic soft actuators. *Adv Mater* **27**, 1668–1675 (2015).
22. Chen HW, Zhang PF, Zhang LW, Liu HL, Jiang Y et al. Continuous directional water transport on the peristome surface of *Nepenthes alata*. *Nature* **532**, 85–89 (2016).
23. Bohn HF, Federle W. Insect aquaplaning: *Nepenthes* pitcher plants capture prey with the peristome, a fully wettable water-lubricated anisotropic surface. *Proc Natl Acad Sci USA* **101**, 14138–14143 (2004).
24. Wong TS, Kang SH, Tang SKY, Smythe EJ, Hatton BD et al. Bioinspired self-repairing slippery surfaces with pressure-stable omniphobicity. *Nature* **477**, 443–447 (2011).
25. Gulfam R, Orejon D, Choi CH, Zhang P. Phase-change slippery liquid-infused porous surfaces with thermo-responsive wetting and shedding states. *ACS Appl Mater Interfaces* **12**, 34306–34316 (2020).
26. Gao CL, Wang L, Lin YC, Li JT, Liu YF et al. Droplets manipulated on photothermal organogel surfaces. *Adv Funct Mater* **28**, 1803072 (2018).
27. Wang J, Sun LY, Zou MH, Gao W, Liu CH et al. Bioinspired shape-memory graphene film with tunable wettability. *Sci Adv* **3**, e1700004 (2017).
28. Li P, Cao MY, Bai HY, Zhao TH, Ning YZ et al. Unidirectional liquid manipulation via an integrated mesh with orthogonal anisotropic slippery tracks. *Adv Funct Mater* **29**, 1904446 (2019).
29. Chen C, Huang ZC, Jiao YL, Shi LA, Zhang YY et al. *In situ* reversible control between sliding and pinning for diverse liquids under ultra-low voltage. *ACS Nano* **13**, 5742–5752 (2019).
30. Lv FY, Zhao F, Cheng DL, Dong ZG, Jia HW et al. Bioinspired functional SLIPSs and wettability gradient surfaces and their synergistic cooperation and opportunities for enhanced condensate and fluid transport. *Adv Colloid Interface Sci* **299**,

102564 (2022).
31. Maeda Y, Lv FY, Zhang P, Takata Y, Orejon D. Condensate droplet size distribution and heat transfer on hierarchical slippery lubricant infused porous surfaces. *Appl Therm Eng* **176**, 115386 (2020).
32. Ma Q, Cui TJ. Information metamaterials: bridging the physical world and digital world. *PhotoniX* **1**, 1 (2020).
33. Qiao Z, Wan ZY, Xie GQ, Wang J, Qian LJ et al. Multi-vortex laser enabling spatial and temporal encoding. *PhotoniX* **1**, 13 (2020).
34. Kim Y, Van Den Berg J, Crosby AJ. Autonomous snapping and jumping polymer gels. *Nat Mater* **20**, 1695–1701 (2021).
35. Manna U, Raman N, Welsh MA, Zayas-Gonzalez YM, Blackwell HE et al. Slippery liquid-infused porous surfaces that prevent microbial surface fouling and kill non-adherent pathogens in surrounding media: a controlled release approach. *Adv Funct Mater* **26**, 3599–3611 (2016).
36. Binks BP, Whitby CP. Silica particle-stabilized emulsions of silicone oil and water: aspects of emulsification. *Langmuir* **20**, 1130–1137 (2004).
37. Horozov TS, Binks BP, Gottschalk-Gaudig T. Effect of electrolyte in silicone oil-in-water emulsions stabilised by fumed silica particles. *Phys Chem Chem Phys* **9**, 6398–6404 (2007).
38. Gonzalez C, Resa JM, Lanz J, Iglesias M, Goenaga JM. Measurements of density and refractive index of soybean oil + short aliphatic alcohols. *Int J Thermophys* **27**, 1463–1481 (2006).
39. Nogueira CA Jr, Carmo FR, Santiago DF, Nogueira VM, Fernandes FAN et al. Viscosities and densities of ternary blends of diesel + soybean biodiesel + soybean oil. *J Chem Eng Data* **57**, 3233–3241 (2012).
40. Žemaitis A, Gaidys M, Brikas M, Gečys P, Račiukaitis G et al. Advanced laser scanning for highly-efficient ablation and ultrafast surface structuring: experiment and model. *Sci Rep* **8**, 17376 (2018).
41. Žemaitis A, Gaidys M, Gečys P, Račiukaitis G, Gedvilas M. Rapid high-quality 3D micro-machining by optimised efficient ultrashort laser ablation. *Opt Lasers Eng* **114**, 83–89 (2019).
42. Zou TT, Zhao B, Xin W, Wang Y, Wang B et al. High-speed femtosecond laser plasmonic lithography and reduction of graphene oxide for anisotropic photoresponse. *Light Sci Appl* **9**, 69 (2020).
43. Zhang YL, Guo L, Xia H, Chen QD, Feng J et al. Photoreduction of graphene oxides: methods, properties, and applications. *Adv Opt Mater* **2**, 10–28 (2014).
44. Jiang HB, Zhao B, Liu Y, Li SY, Liu J et al. Review of photoreduction and synchronous patterning of graphene oxide toward advanced applications. *J Mater Sci* **55**, 480–497 (2020).
45. Smith JD, Dhiman R, Anand S, Reza-Garduno E, Cohen RE et al. Droplet mobility on lubricant-impregnated surfaces. *Soft Matter* **9**, 1772–1780 (2013).
46. Furmidge CGL. Studies at phase interfaces. I. The sliding of liquid drops on solid surfaces and a theory for spray retention. *J Colloid Sci* **17**, 309–324 (1962).
47. Dai XM, Stogin BB, Yang SK, Wong TS. Slippery wenzel state. *ACS Nano* **9**, 9260–9267 (2015).
48. Zhang SN, Huang JY, Chen Z, Lai YK. Bioinspired special wettability surfaces: from fundamental research to water harvesting applications. *Small* **13**, 1602992 (2017).
49. Han DD, Zhang YL, Jiang HB, Xia H, Feng J et al. Moisture-responsive graphene paper prepared by self-controlled photoreduction. *Adv Mater* **27**, 332–338 (2015).
50. Han DD, Zhang YL, Liu Y, Liu YQ, Jiang HB et al. Bioinspired graphene actuators prepared by unilateral UV irradiation of graphene oxide papers. *Adv Funct Mater* **25**, 4548–4557 (2015).
51. Liu YQ, Chen ZD, Han DD, Mao JW, Ma JN et al. Bioinspired soft robots based on the moisture-responsive graphene oxide. *Adv Sci* **8**, 2002464 (2021).
52. You R, Liu YQ, Hao YL, Han DD, Zhang YL et al. Laser fabrication of graphene-based flexible electronics. *Adv Mater* **32**, 1901981 (2020).
53. Žemaitis A, Mimidis A, Papadopoulos A, Gečys P, Račiukaitis G et al. Controlling the wettability of stainless steel from highly-hydrophilic to super-hydrophobic by femtosecond laser-induced ripples and nanospikes. *RSC Adv* **10**, 37956–37961 (2020).
54. Zhang YL, Liu YQ, Han DD, Ma JN, Wang D et al. Quantum-confined-superfluidics-enabled moisture actuation based on unilaterally structured graphene oxide papers. *Adv Mater* **31**, 1901585 (2019).
55. Xu WH, Zhou XF, Hao CL, Zheng HX, Liu Y et al. SLIPS-TENG: robust triboelectric nanogenerator with optical and charge transparency using a slippery interface. *Natl Sci Rev* **6**, 540–550 (2019).
56. Indrišiūnas S, Voisiat B, Gedvilas M, Račiukaitis G. New opportunities for custom-shape patterning using polarization control in confocal laser beam interference setup. *J Laser Appl* **29**, 011501 (2017).
57. Gedvilas M, Voisiat B, Indrišiūnas S, Račiukaitis G, Veiko V et al. Thermo-chemical microstructuring of thin metal films using multi-beam interference by short (nano- & picosecond) laser pulses. *Thin Solid Films* **634**, 134–140 (2017).

Acknowledgements

The authors acknowledge the National Natural Science Foundation of China (NSFC) under Grant Nos. #61905087, and #61935008. Tsinghua University (School of Materials Science and Engineering)-AVIC Aerodynamics Research Institute Joint Research Center for Advanced Materials and Anti-Icing Nos. #JCAMAI-2020-03. Fundamental Research Funds for the Central Universities Nos. #2020-JCXK-18. Jilin Province Development and Reform Commission Project Nos. #2022C047-4. Key Laboratory of Icing and Anti/De-icing of CARDC Nos. # IADL 20210404.

Competing interests

The authors declare no competing financial interests.

Supplementary information

Supplementary information is available for this paper at https://doi.org/10.29026/oea.2023.210163